Cerebral Blood Flow MRI in Mice Using the Cardiac-Spin-Labeling Technique

Eric R. Muir, Qiang Shen, and Timothy Q. Duong*

Continuous arterial spin labeling MRI with a separate neck labeling coil provides a highly sensitive method to image cerebral blood flow (CBF). In mice, however, this has not been possible because the proximity of the neck coil to the brain uses the neck coil to significantly saturate the brain signal. To overcome this limitation the cardiac spin labeling (CSL) technique is introduced in which the labeling coil is placed at the heart position. To demonstrate its utility, CSL CBF was applied to image quantitative basal CBF and hypercapnia-induced CBF changes. This approach provides a practical means to image CBF with high sensitivity in small animals, compares favorably to existing mouse CBF imaging techniques, and could broaden CBF applications in mice where many brain disease and transgenic models are widely available. Magn Reson Med 60: 744–748, 2008. © 2008 Wiley-Liss, Inc.

Key words: CBF; arterial spin labeling; fMRI; mouse

Cerebral blood flow (CBF) is tightly regulated and intricately coupled to basal metabolic function under normal physiologic conditions. Perturbations of basal CBF and stimulus-evoked CBF responses have been implicated in many neurological diseases such as stroke, brain tumor, and neurodegeneration. CBF MRI is becoming increasingly popular because it is noninvasive and has high spatial resolution. CBF MRI commonly employs: 1) the dynamic susceptibility contrast (DSC) technique by administering a bolus of an exogenous intravascular contrast agent, or 2) the arterial spin labeling (ASL) technique by magnetically labeling the endogenous water in the in-flowing blood (see review, Ref. 1). The DSC technique is efficient but has relatively low spatial resolution and is incompatible with real-time CBF functional MRI (fMRI) measurements because the long half-life of the exogenous contrast agent allows only one measurement per bolus injection. ASL, on the other hand, allows multiple repeated CBF measurements because the magnetically labeled water has a favorable short half-life (blood T_1 of ≈2.0 sec), which can be used for dynamic fMRI measurements, augmentation of spatial resolution, and/or signal-to-noise ratio (SNR).

ASL can be performed using the same coil or separate coils for labeling and imaging. The latter approach yields improved CBF SNR because magnetization-transfer effect is avoided. While continuous ASL using a separate neck labeling coil is commonly employed in rats (2), humans (3), and monkeys (4), its extension to mice has not been possible because the proximity of the neck coil and the brain coil (≈1 cm from center to center) results in significant saturation of the brain signal by the neck coil, causing significant CBF measurement errors. This occurs even when the coils are actively decoupled, coil sizes are minimized, and the intercoil distance is maximized. CBF using other MRI techniques in mice is sparse; only a few CBF studies using the single-coil ASL method (5,6) and the DSC method (7) have been reported.

This study introduces a practical means to overcome the above limitations. This approach is referred to as the cardiac spin labeling (CSL) technique in which continuous spin labeling is performed with a separate labeling coil placed at the heart position to avoid saturation of the brain signal. To demonstrate its utility, multislice echo-planar-imaging was employed to image quantitative basal CBF and CBF fMRI associated with hypercapnic challenge.

MATERIALS AND METHODS

Animal Preparations

Mice (C57BL6, 21–28 g, 6–10 weeks, $n = 9$) were imaged under ≈1.2% isoflurane and spontaneous breathing conditions. Measurements of labeling efficiency, CBF, and hypercapnia-induced CBF changes were made. Animals were placed in a custom-made animal holder with ear and mouth bars. Respiration rate (80–130 bpm) and rectal temperature (37 ± 0.5°C) were continuously monitored and maintained within normal physiological ranges unless otherwise perturbed. All mice recovered from anesthesia at the end of the MRI, lasting up to 4 hr, during which multiple measurements were made.

Hypercapnic Challenges

Hypercapnic challenge used a premixed gas of 5% CO_2 with 30% O_2 and balance N_2. The baseline was 30% O_2 with balance N_2 to ensure proper oxygenation under anesthesia. Each trial consisted of 3.5-min baseline and 3.5-min hypercapnia. A 10-min break was given between trials for the animals to return to normal physiologic conditions (8). Two to four repeated measurements for each gas condition were typically made.

MRI Methods

MRI studies were performed on a 7 T/30 cm magnet and a 150 G/cm B-GA6S gradient insert (Bruker, Billerica, MA). Mice were placed onto a head holder consisting of ear and tooth bars. A small circular surface coil (ID = 1.1 cm) was placed on top of the head. A circular labeling coil (ID = 0.8 cm), built into the cradle, was placed at the heart

Yerkes Imaging Center, Department of Neurology, Emory University, Atlanta, Georgia.

Grant sponsor: National Institutes of Health / National Institute of Neurological Disorders and Stroke (NIH/NINDS); Grant number: R01-NS45879; Grant number: Venture Grant NIH P50 AG025688.

*Correspondence to: Timothy Q. Duong, PhD, Yerkes Imaging Center, Emory University, 954 Gatewood Rd. NE, Atlanta, GA 30329. E-mail: tduong@emory.edu

Received 15 January 2008; revised 12 April 2008; accepted 13 May 2008.
DOI 10.1002/mrm.21721
Published online in Wiley InterScience (www.interscience.wiley.com).

position for continuous CSL. The two coils were positioned parallel to each other, separated by 2 cm from center to center, and were actively decoupled.

Labeling efficiency was measured using conventional gradient-echo acquisition with field of view (FOV) = 1.1 × 0.8 cm or 1.1 × 1.1 cm, matrix = 128 × 128, slice thickness = 1 mm, TE = 4.57 ms, 1 slice, labeling duration = 300 ms, 5–7 variable powers, and a TR = 313 ms. The short TR was used to saturate static brain signal for better delineation of the blood vessels, while steady-state labeling could still be achieved in large arteries.

Blood-flow MRI was acquired using the CSL technique with gradient-echo EPI. Paired images were acquired in an interleaved fashion. The continuous CSL employed a 2.1-sec square RF pulse to the labeling coil in the presence of 2.0 G/cm gradient (2,9). The sign of the frequency offset was switched for nonlabeled images. The other MRI parameters were: FOV = 1.28 × 1.28 cm, matrix = 64 × 64 (single-shot EPI) or 128 × 128 (four-shot EPI), slice thickness = 1 mm, 9 slices, labeling duration = 2.1 sec, TR = 2.6 sec per segment, and TE = 10 ms.

Data Analysis

Image analysis employed codes written in MatLab (MathWorks, Natick, MA) and STIMULATE software (University of Minnesota). Basal CBF data were derived from measurements before physiologic stimulations.

Labeling efficiency was calculated from the arrayed labeling power data using $\alpha = (S_{NL} - S_L)/(2\ S_{NL})$, where S_{NL} and S_L are the signal intensities in the arteries of the nonlabeled images and labeled images, respectively, with the optimal labeling power. The optimal labeling power was obtained when the arterial signals reached plateau with increasing power. The vessels employed for the labeling efficiency calculations were the distal internal carotid arteries at the base of frontal lobe. Blood-flow signals (S_{CBF}) in the brain with intensity in units of mL/g/min were calculated using $S_{CBF} = \lambda/T_1\ [(S_{NL}\text{-}S_L)/(S_L+(2\alpha\text{-}1)S_{NL})]$ (9), where S_{NL} and S_L are signal intensities of the nonlabeled and labeled images, respectively. λ, the water tissue–blood partition coefficient, was taken to be 0.9, and whole-brain T_1 at 7 T was taken to be 1.7 sec (9). The labeling efficiency α was measured to be 0.73 (see Results).

CBF fMRI percent changes in the response to hypercapnia were analyzed. Quantitative CBF analysis employed regions of interest (ROIs), including the whole brain, frontal cortex, sensory-motor cortex, corpus callosum, hippocampus, caudate putamen, thalamus, inferior colliculus, superior colliculus, pons, and cerebellum.

RESULTS

The schematic of the CSL setup is shown in Fig. 1. The optimal peak-to-peak labeling power, measured at the connection to the RF coil accounting for attenuation of the long RF cable, was 6 mW. Given the low power employed and highly perfused heart tissue, heating is not expected to be an issue. Labeling efficiency was determined to be 0.73 ± 0.06 (n = 5), measured at the distal internal carotid arteries at the base of frontal lobe.

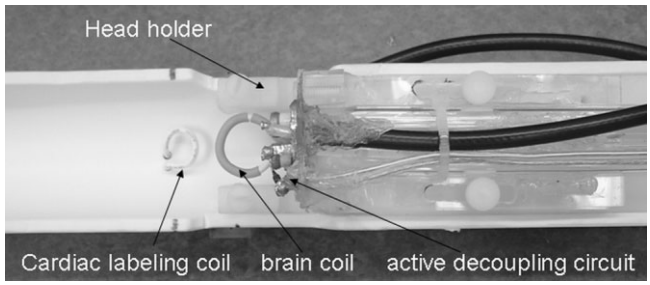

FIG. 1. Schematics of the cardiac spin labeling setup. The cardiac labeling coil and the brain coil are separated by 2 cm from center to center.

Quantitative CBF images at 200 × 200 × 1000 μm (Fig. 2A) and 100 × 100 × 1000 μm (Fig. 2B) show heterogeneous blood-flow contrast, as expected. CBF is lower in the corpus callosum (white matter) compared to gray matter. Note that CBF in the cerebellum and brain stem could be imaged, in contrast to two-coil ASL CBF in rats where the cerebellum and brain stem are often not reported due to saturation artifacts by the neck labeling coil. The whole-brain CBF was 1.07 ± 0.08 mL/g/min (n = 5). Regional CBF values, obtained from different ROIs (shown in Fig. 2C) are summarized in Table 1. The CBF fMRI time course responding to hypercapnic challenge from a single measurement from one animal is shown in Fig. 3. The group-averaged hypercapnia-induced CBF percent change was 33 ± 16% (n = 5).

DISCUSSION

This study demonstrates a practical approach to image quantitative CBF and physiologically evoked CBF changes in mice using the continuous spin labeling technique with a cardiac labeling coil. This CSL CBF technique overcomes existing limitations and offers the following advantages: 1) Multislice high-resolution CBF images and CBF fMRI can be obtained with high sensitivity without magnetization-transfer effect. 2) The distance between the heart and the brain in mice (≈2 cm) avoids saturation of the brain signal by the label coil. 3) CBF of the cerebellum and brain stem could be imaged in contrast to two-coil ASL CBF in rats where the cerebellum and brain stem are often not reported due to saturation artifacts by the neck labeling coil. Moreover, CBF MRI in other body parts within reasonable transit time, such as the kidneys and liver, might be possible. 4) Finally, decoupling circuitry may be unnecessary for CSL CBF MRI given the distance between the two coils, especially in rats. In sum, CSL CBF MRI has the potential to broaden CBF MRI utility in mice and other similar size species.

Potential Errors in Absolute CBF Values

Quantitative CBF measurement by MRI is susceptible to errors, which include magnetization-transfer, transit-time, and water-exchange effect (see review, Ref. 1). Magnetization-transfer effect was not an issue for cASL herein because a separate labeling coil was used and all RF coils

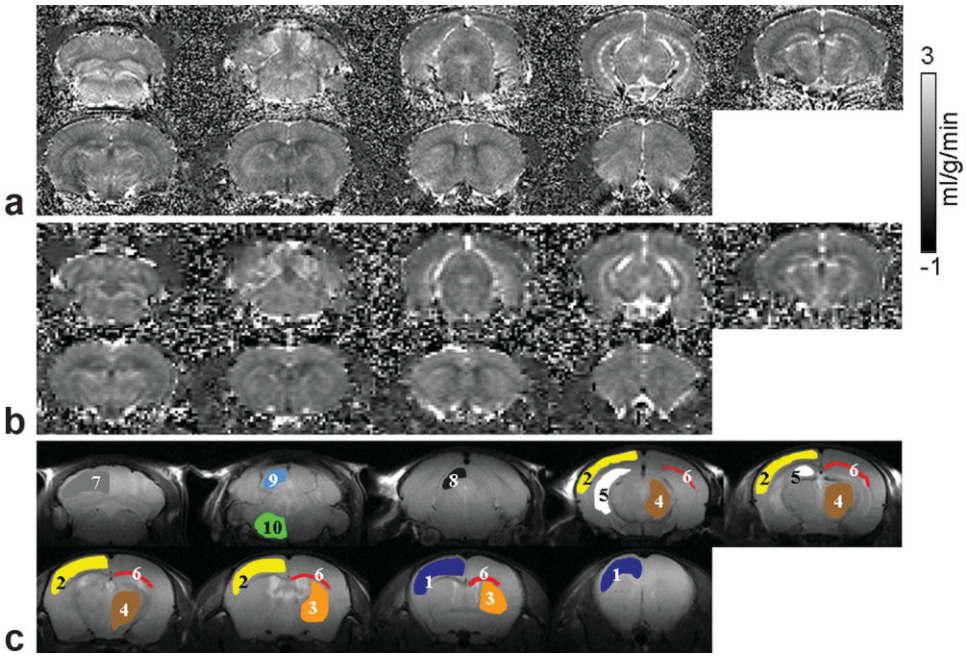

FIG. 2. Multislice CBF image at **(a)** 200 × 200 × 1000 μm and **(b)** 100 × 100 × 1000 μm. **c:** ROIs overlaid on anatomical CBF image used for regional CBF analysis: 1. frontal cortex; 2. sensory-motor cortex; 3. caudate putamen; 4. thalamus; 5. hippocampus; 6. corpus callosum; 7. cerebellum; 8. superior colliculus; 9. inferior colliculus; 10. pons.

were actively decoupled. In almost all ASL measurements to date, including ours, a single arterial transit time was used because of the difficulty in obtaining it in an image form and CBF is weakly dependent on arterial transit times within the physiologic ranges. Because of the sequential multislice acquisition, different image slices may have a slightly different transit time. The water-exchange effect on CBF quantification is complex, depending on the precise difference between blood T_1 and tissue T_1, blood flow values, the extent of water exchange, magnetic field strength, CBF measurement techniques, and CBF calculation models, among others. Some of these effects counterbalance each other. In this study we employed a widely used single-compartment CBF quantification model that ignores water exchange. Improving absolute CBF quantification remains an active area of research.

Cross-validation with other techniques, such as microsphere and iodoantipyrine, may be helpful but was not performed here. These techniques are also susceptible to errors such as particle size, concentration, and postmortem artifacts, among others.

Table 1
Mouse CBF in Different Brain Regions (Mean ± SD, n = 5)

Region of interest (ROI)	CBF (ml/g/min)
Whole brain	1.07 ± 0.08
Frontal cortex	1.00 ± 0.14
Sensory-Motor cortex	0.92 ± 0.14
Caudate putamen	1.08 ± 0.06
Thalamus	1.18 ± 0.08
Hippocampus	1.28 ± 0.08
Corpus callosum	0.53 ± 0.10
Cerebellum	1.08 ± 0.15
Superior colliculus	1.18 ± 0.15
Inferior colliculus	1.51 ± 0.42
Pons	1.40 ± 0.21

Labeling Efficiency

Our labeling efficiency of 0.73 ± 0.06 is consistent with the majority of published data, namely: 0.7 (3) at 1.5–3 T, 0.75 at 4.7 T (10), and 0.8 at 9.4 T (11). The labeling efficiency in our study was measured at the imaging plane (as opposed to the carotid arteries in the neck), and thus labeling efficiency takes into account the transit time. This approach avoids the need for measuring transit time, which is difficult to measure using ASL.

In our initial measurements of labeling efficiency in the carotid arteries under the cerebellum, the labeling efficiency was surprisingly low (≈0.63). Labeling efficiency was measured at three different slice positions from the carotid arteries under the cerebellum to the distal internal carotid arteries under the frontal lobe (covering ≈7 mm range). Contrary to expectation, labeling efficiencies increased from 0.63 at the carotid arteries under the cerebellum to 0.73 at the distal internal carotid arteries in the

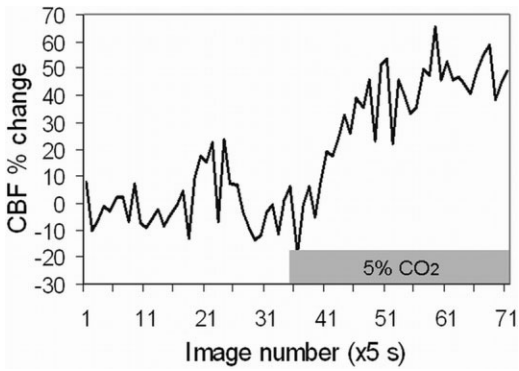

FIG. 3. Whole-brain CBF time course responding to 5% CO_2 (30% O_2 + balance N_2) relative to baseline (30% O_2 + balance N_2) from a single measurement in one mouse.

middle and frontal slices. This observation indicated that there were saturation effects by the cardiac labeling coil due to proximity. Thus, it is important that labeling efficiency be measured at the distal internal carotid arteries under the frontal lobe, which was verified to have no saturation effect from the cardiac labeling coil in our setup.

Quantitative CBF

The whole-brain CBF in mice was 1.07 ± 0.08 mL/g/min under 1.2% isoflurane. Our quantitative CBF in mice is consistent with CBF values in rats, which ranged from 0.76 to 1.1 mL/g/min (8,12), obtained using continuous ASL MRI with a separate neck coil under essentially identical experimental conditions. Quantitative CBF measurements in mice have also been reported using destructive techniques, predominantly measured using iodoantipyrine autoradiography and microsphere, and these CBF values were 0.78–1.25 mL/g/min under ketamine/xylazine (13) and 0.5–1.0 mL/g/min under equithesin anesthesia (14). Our results are in reasonable agreement despite different anesthetics.

However, our CBF values in mice are slightly lower than those in mice obtained using the single-coil ASL technique, which reported 1.7–2.8 mL/g/min under 2% isoflurane (6) and 1.5–2.0 mL/g/min under 1% halothane (5) among different brain regions. These single-coil approaches imaged one slice at comparatively lower spatial resolution. It is important to note that isoflurane is a known vasodilator. Previous studies have shown that rat CBF under 1% isoflurane anesthesia was substantially higher than under awake conditions in the same animals (15) and under α-chloralose in separate animals (16). Moreover, increasing isoflurane from 1% to 2% has been reported to increase CBF from 0.87 ± 0.27 to 1.31 ± 0.30 mL/g/min in the same animals (17). Halothane has been reported to be have a stronger vasodilatory effect than isoflurane (18). In short, the minor discrepancy between our value and single-coil ASL technique could be due to technique (including CBF model equation) and anesthetics.

CBF fMRI of Hypercapnic Challenge

The CBF percent change was 33 ± 16%. We did not find similar mouse CBF fMRI studies for comparison. Hypercapnia-induced CBF changes in mice on the artificial surface, as measured by laser speckle flowmetry, have been reported to increase 40–55% under α-chloralose and 15% under 1% isoflurane (19), and 60–75% under urethane/α-chloralose (20). In rats, hypercapnia-induced CBF increase has been reported as 60%, using MRI (8) and under essentially identical experimental conditions. Similar hypercapnia-induced CBF increases have also been reported in awake humans. Our hypercapnia-induced CBF increases in mice are comparable to those made in mice using laser speckle flowmetry. The change is slightly low compared to measurements made under different anesthetics and in rats using MRI. This may be explained by the use of isoflurane, which attenuates vascular responses (19).

CONCLUSIONS

This study demonstrates a simple and practical approach to image CBF in mice using a separate cardiac labeling coil. Whole-brain CBF, including those of the cerebellum and brain stem, can be imaged. The SNR, spatiotemporal resolution, multislice, and fMRI capability of CSL CBF MRI compares favorably with existing approaches for mice. This approach could provide a valuable tool to study numerous brain disease and transgenic models available in small animals, including stroke and Alzheimer's disease.

REFERENCES

1. Calamante F, Thomas DL, Pell GS, Wiersma J, Turner R. Measuring cerebral blood flow using magnetic resonance imaging techniques. J Cereb Blood Flow Metab 1999;19:701–735.
2. Williams DS, Detre JA, Leigh JS, Koretsky AP. Magnetic resonance imaging of perfusion using spin inversion of arterial water. Proc Natl Acad Sci USA 1992;89:212–216.
3. Talagala SL, Ye FQ, Ledden PJ, Chesnick S. Whole-brain 3D perfusion MRI at 3.0 T using CASL with a separate labeling coil. Magn Reson Med 2004;52:131–140.
4. Zhang X, Nagaoka T, Auerbach EJ, Champion R, Zhou L, Hu X, Duong TQ. Quantitative basal CBF and CBF fMRI of rhesus monkeys using three-coil continuous arterial spin labeling. Neuroimage 2007;34:1074–1083.
5. van Dorsten FA, Hata R, Maeda K, Franke C, Eis M, Hossmann KA, Hoehn M. Diffusion- and perfusion-weighted MR imaging of transient focal cerebral ischaemia in mice. NMR Biomed 1999;12:525–534.
6. Foley LM, Hitchens TK, Kochanek PM, Melick JA, Jackson EK, Ho C. Murine orthostatic response during prolonged vertical studies: effect on cerebral blood flow measured by arterial spin-labeled MRI. Magn Reson Med 2005;54:798–806.
7. Koistinaho M, Kettunen MI, Goldsteins G, Keinanen R, Salminen A, Ort M, Bures J, Liu D, Kauppinen RA, Higgins LS, Koistinaho J. Beta-amyloid precursor protein transgenic mice that harbor diffuse A beta deposits but do not form plaques show increased ischemic vulnerability: role of inflammation. Proc Natl Acad Sci U S A 2002;99:1610–1615.
8. Sicard KM, Duong TQ. Effects of hypoxia, hyperoxia and hypercapnia on baseline and stimulus-evoked BOLD, CBF and CMRO2 in spontaneously breathing animals. Neuroimage 2005;25:850–858.
9. Shen Q, Ren H, Cheng H, Fisher M, Duong TQ. Functional, perfusion and diffusion MRI of acute focal ischemic brain injury. J Cereb Blood Flow Metab 2005;25:1265–1279.
10. Shen Q, Meng X, Fisher M, Sotak CH, Duong TQ. Pixel-by-pixel spatiotemporal progression of focal ischemia derived using quantitative perfusion and diffusion imaging. J Cereb Blood Flow Metab 2003;23:1479–1488.
11. Silva AC, Kim SG, Garwood M. Imaging blood flow in brain tumors using arterial spin labeling. Magn Reson Med 2000;44:169–173.
12. Liu ZM, Schmidt KF, Sicard KM, Duong TQ. Imaging oxygen consumption in forepaw somatosensory stimulation in rats under isoflurane anesthesia. Magn Reson Med 2004;52:277–285.
13. LaRue B, Hogg E, Sagare A, Jovanovic S, Maness L, Maurer C, Deane R, Zlokovic BV. Method for measurement of the blood-brain barrier permeability in the perfused mouse brain: application to amyloid-beta peptide in wild type and Alzheimer's Tg2576 mice. J Neurosci Methods 2004;138:233–242.
14. de Vasconcelos AP, Bouilleret V, Riban V, Wasterlain C, Nehlig A. Role of nitric oxide in cerebral blood flow changes during kainate seizures in mice: genetic and pharmacological approaches. Neurobiol Dis 2005;18:270–281.
15. Sicard K, Shen Q, Brevard ME, Sullivan R, Ferris CF, King JA, Duong TQ. Regional cerebral blood flow and BOLD responses in conscious and anesthetized rats under basal and hypercapnic conditions: implications for functional MRI studies. J Cereb Blood Flow Metab 2003;23:472–481.
16. Duong TQ, Silva AC, Lee SP, Kim SG. Functional MRI of calcium-dependent synaptic activity: cross correlation with CBF and BOLD measurements. Magn Reson Med 2000;43:383–392.

17. Duong TQ, Iadecola C, Kim SG. Effect of hyperoxia, hypercapnia, and hypoxia on cerebral interstitial oxygen tension and cerebral blood flow. Magn Reson Med 2001;45:61–70.
18. Drummond JC, Scheller MS, Todd MM. The effect of nitrous oxide on cortical cerebral blood flow during anesthesia with halothane and isoflurane, with and without morphine, in the rabbit. Anesth Analg 1987;66:1083–1089.
19. Ayata C, Dunn AK, Gursoy-Ozdemir Y, Huan Z, Boas DA, Moskowitz MA. Laser speckle flowmetry for the study of cerebrovascular physiology in normal and ischemic mouse cortex. J Cereb Blood Flow Metab 2004;24:744–755.
20. Niwa K, Carlson GA, Iadecola C. Exogenous A beta1–40 reproduces cerebrovascular alterations resulting from amyloid precursor protein overexpression in mice. J Cereb Blood Flow Metab 2000;20:1659–1668.